JOURNAL OF BACTERIOLOGY, Mar. 1997, p. 1671–1683 Vol. 179, No. 5
0021-9193/97/$04.00+0

The *divIVA* Minicell Locus of *Bacillus subtilis*

JEONG-HEON CHA[1]† AND GEORGE C. STEWART[2]*

Department of Microbiology and Immunology, University of South Carolina School of Medicine, Columbia, South Carolina,[1] and Department of Diagnostic Medicine/Pathobiology, College of Veterinary Medicine, Kansas State University, Manhattan, Kansas[2]

Received 23 September 1996/Accepted 13 December 1996

The *Bacillus subtilis divIVA1* mutation causes misplacement of the septum during cell division, resulting in the formation of small, circular, anucleate minicells. This study reports the cloning and sequence analysis of 2.4 kb of the *B. subtilis* chromosome including the *divIVA* locus. Three open reading frames were identified: *orf*, whose function is unknown; *divIVA*; and isoleucyl tRNA synthetase (*ileS*). We identified the point mutation in the *divIVA1* mutant allele. Inactivation of *divIVA* produces a minicell phenotype, whereas overproduction of DivIVA results in a filamentation phenotype. Mutants with mutations at both of the minicell loci of *B. subtilis*, *divIVA* and *divIVB*, possess a minicell phenotype identical to that of the DivIVB$^-$ mutant. The DivIVA$^-$ mutants, but not the DivIVB$^-$ mutants, show a decrease in sporulation efficiency and a delay in the kinetics of endospore formation. The data support a model in which *divIVA* encodes the topological specificity subunit of the *minCD* system. The model suggests that DivIVA acts as a pilot protein, directing *minCD* to the polar septation sites. DivIVA also appears to be the interface between a sporulation component and MinCD, freeing up the polar septation sites for use during the asymmetric septation event of the sporulation process.

Bacillus subtilis is a gram-positive rod-shaped endospore-forming soil bacterium. Like other rod-shaped bacteria, this bacterium replicates by a process in which the cell doubles its mass by doubling its length and then divides into two daughter cells. The division process is highly regulated both temporally and spatially. Temporal regulation ensures that chromosomal replication and segregation precede cytokinesis and spatial regulation results in the division septum forming at the central site of the cell, equidistant from the cell poles. The cellular architecture which defines a septation site remains one of the most significant unanswered questions left in procaryotic biology. It is known that bacterial cell division can occur at sites other than the cell midpoint. Minicell-producing divisions have been described for mutant cells of both *Escherichia coli* and *Bacillus subtilis* (1, 21, 27, 32). Minicells are small, generally spherical, anucleate cells produced by a septation event occurring near one pole of the bacterial cell, rather than at the midpoint. Studies utilizing minicell mutants have indicated that there are three potential septation sites in a rod-shaped cell. One is the normal division site at the midpoint of the cell, and two polar sites occur near the ends of the cell. The latter sites are utilized in the minicell divisions. Pioneering work by Rothfield and coworkers has elucidated the mechanism of the regulation of septum site selection by the *minB* operon of *E. coli* (12). The *minB* operon encodes three genes, designated *minCDE*. The MinC and MinD proteins function as an inhibitor of septation which is capable of blocking division at all three potential division sites. The former is the actual inhibitor, whereas MinD is the regulatory subunit of the pair. It has ATPase activity and confers on MinC the capacity to function at physiological levels of the protein (11, 13, 14). MinE is a small protein which is the topological specificity subunit preventing inhibition of septation by MinCD at the midcell sites. The MinE protein has two functional domains: the N-terminal part of the 88-amino-acid protein functions to counteract the MinCD inhibitor, whereas the C-terminal domain confers topological specificity (29, 45). The MinCD inhibitor appears to act by interfering with the function of the essential cell division protein FtsZ (5). Production of minicells in *E. coli* can also be induced by moderate overproduction of FtsZ (43).

Mutations at one of three loci in *B. subtilis* 168 are associated with a minicell phenotype: *divIVA*, located at 144° on the genetic map; *divIVB*, located at 245°; and *divIVC*, at 15° (27, 37). However, there has been no follow-up study on *divIVC*, as the mutant apparently no longer exists. The *divIVB* locus has been cloned, sequenced, and characterized by three different groups (23, 26, 39). The *divIVB* locus contains five genes arranged in two functionally distinct gene clusters (*mre* and *min*) and transcribed as a single unit. The first gene cluster contains three genes (*mreBCD*) homologous to the *mre* cell shape determination genes of *E. coli* (15, 40, 41). The *min* gene cluster has two minicell genes, *minC* and minD, inactivation of either of which induces a minicell phenotype in *B. subtilis*. Surprisingly, a *B. subtilis* homolog of *E. coli minE* is not present in the *divIVB* operon, and the topological specificity-conferring subunit must be located elsewhere on the *B. subtilis* chromosome.

An added complexity to the septum site selection system in *B. subtilis* is the sporulation process. During endospore formation, an asymmetric septation event occurs which results in the establishment of the forespore and mother cell compartments. This sporulation-associated septation event apparently utilizes the polar septation site of the *minCD*-regulated system and additionally involves genes whose products are essential for vegetative growth-associated cell division such as *ftsA*, *ftsZ*, and *divIC* (3–5, 24). The requirement for the septum site selection system to interface with the sporulation machinery may explain a chromosomal location of the *minE* homolog separate from *minCD*.

The *divIVA* locus has been proposed to be the site of the missing *minE* determinant (33). The *divIVA1* minicell mutant was originally isolated and characterized by Reeve et al. (32). The *divIVA1* strain differs from the *divIVB1* strain in that it produces fewer minicells and is more filamentous, whereas the

* Corresponding author. Mailing address: Department of Diagnostic Medicine/Pathobiology, College of Veterinary Medicine, Kansas State University, Manhattan, KS 66506. Phone: (913) 532-4419. Fax: (913) 532-4039. E-mail: stewart@vet.ksu.edu.

† Present address: Department of Microbiology, University of Texas Southwestern Medical Center, Dallas, TX 75235.

TABLE 1. Bacterial strains used in this study

Strain	Genotype	Source and/or reference
B. subtilis 168		
CU403-*divIVA1*	*ilvD divIVA1 thyA thyB*	J. N. Reeve 32
CU4130	*pyr-83*::Tn*917 trpC2*	BGSC[a]
CU4153	*trpC2 zdi-82*::Tn*917*	BGSC
JH158	*cysC1 trpC2*	BGSC
KSS1001	*trpC2*	39
KSS1067	*trpC2 zdi-82*::*21*Δ*2*	This work
KSS1101	*divIVB1 trpC2*	39
KSS1168	*divIVA1 trpC2*	This work
KSS1178	*minC*::pAV2210 *trpC2*	39
KSS1180	*pyr-83*::*21*Δ*2 trpC2*	This work
KSS1182	*trpC2* (pTW880)	42
KSS1200	JH158ΩpCHA2392	This work
KSS1207	KSS1001ΩpCHA2421	This work
KSS1227	KSS1001ΩpCHA2468	This work
KSS1230	KSS1168ΩpCHA2469	This work
KSS1232	KSS1001ΩpCHA2475	This work
KSS1237	KSS1001*divIVA*::*cat* (at *Eco*RI)	This work
KSS1248	KSS1001 *divIVA*::*cat* (at *Sal*I)	This work
KSS1254	KSS1001 *divIVA*::Pm^r (at *Eco*RI)	This work
KSS1258	KSS1254(pCHA2542)	This work
KSS1261	*divIVA1 minC*::pAV2210 *trpC2*	This work
KSS1262	*divIVA1*::Pm^r *trpC2*	This work
KSS1263	*minC*::pAV2210 *divIVA*::Pm^r *trpC2*	This work
KSS1264	KSS1101(pCHA2542)	This work
KSS1266	KSS1168(pCHA2542)	This work
SUIII	*thyA thyB trpC2 ts1* [*ftsZ*(Ts)]	R. G. Wake
E. coli		
ABLE K	*hsdR* (r_K^- m_K^-) Kan^r *lacZ*ω *mcrA mcrCB mcrF mrr* F′ *proAB lacI*^{q}ZΔM15 Tn*10*	Stratagene
KE94	*ara-14 galK2 hsdS20 lacY1 mtl-1 pcnB20 proA2 recA13 rpsL20 supE44 xyl-5 zad*::Tn*10*	31
DH5α	*endA1 gyrA96 hsdR17* Δ(*lacZYA-argF*)*U169 recA1 supE44 thi-1* ϕ80d*lacZ*ΔM15	Promega
LE392	*galK2 galT22 hsdR514 lacY1 metB1 supE44 supF58 trpR55*	Promega

[a] BGSC, *Bacillus* Genetic Stock Center, Ohio State University, Columbus.

divIVB1 mutant strain produces at greater frequency not only spherical minicells but also extremely short rods of varying length (32).

In this paper, we report the cloning and characterization of the *divIVA* determinant of *B. subtilis*. The *divIVA* determinant has been identified, and the nature of the *divIVA1* allele has been elucidated. The effects of DivIVA on vegetative cell division and sporulation were evaluated, and a model for DivIVA function is proposed.

MATERIALS AND METHODS

Bacterial strains, plasmids, and growth conditions. The bacterial strains used in this study are listed in Table 1. Because of a competence defect in CU403-*divIVA1*, the *divIVA1* mutant allele was moved into a more competence-proficient background by transforming JH158 with chromosomal DNA from CU403-*divIVA1* and selecting for *cysC*$^+$ transformants. Cotransformation of the *divIVA1* allele was screened for by phase-contrast microscopic examination of individual colonies for the presence of minicells. The resulting transformant, KSS1168, became highly competent and was used for all subsequent manipulations involving *divIVA1*. *E. coli* KE94 and ABLE K were used when low plasmid copy numbers were required. Plasmids used in this study are listed in Table 2.

Media and growth conditions for *E. coli* and *B. subtilis* were as described previously (22, 35). Phleomycin was utilized at 10 and 7 μg/ml for selection with *E. coli* and *B. subtilis*, respectively; kanamycin was utilized at 20 and 5 μg/ml for selection with *E. coli* and *B. subtilis*, respectively; and spectinomycin was utilized at a concentration of 100 μg/ml.

General methods. Competent *E. coli* and *B. subtilis* cells were prepared and transformed as described by Dagert and Ehrlich and by Erickson and Copeland, respectively (10, 16). Plasmid DNA from *E. coli* was prepared by the alkaline lysate procedure of Birnboim and Doly (6). Isolation of chromosomal and plasmid DNAs from *B. subtilis* was performed as described previously (22, 34).

DNA methods. Southern blots, colony blots, and hybridization conditions were as previously described (7, 22). Radiolabeled DNA probes were prepared by the random priming method (17). Nucleotide sequence determination was carried out with the *fmol* sequencing kit (Promega) and ^{35}S-dATP (DuPont). Both DNA strands were completely sequenced.

Chromosomal walking to *divIVA*. Tn*917*-bearing strains of *B. subtilis* (38) were screened for transposon insertions linked to *divIVA*. A Tn*917* transposon linked to *divIVA* was replaced with the pTV21Δ2 element by the method of Youngman et al., thus replacing *erm* and the transposition competency of Tn*917* by the Cm^r replicon of pTV21Δ2 (44). The pTV21Δ2/Tn*917* exchanges were confirmed by Southern blot hybridization analysis (8). The resulting transformants, KSS1180 and KSS1067 (Fig. 1), were constructed from CU4130 and CU4153, respectively. KSS1168 was transformed to Cm^r with the chromosomal DNA from KSS1067 or KSS1180 and subsequently screened for the *divIVA*$^+$ phenotype.

For chromosomal walking in the leftward direction as depicted in Fig. 1, pCHA2346 was constructed as an *Eco*RI excision from KSS1180 chromosomal DNA and is identical to pQS31 as described by Quinn et al. (31). pCHA2346 contains 7.4 kb of *B. subtilis* chromosomal DNA producing a 12-kb plasmid. The 0.85-kb *Eco*RI-*Bgl*II DNA fragment from the insert terminus of pCHA2346 was subcloned into pUK19 to produce pCHA2361. However, attempts to integrate pCHA2361 into the *B. subtilis* chromosome failed. Insertion of the plasmid at this site results in an apparent loss of viability. Sequence of this 0.85-kb *Eco*RI-*Bgl*II fragment revealed that it lies wholly internally to the isoleucyl tRNA synthetase (*ileS*) gene (8). Integration of pCHA2361 would therefore result in a lethal disruption of this essential determinant. Therefore, the nearby 1.84-kb *Cla*I-(upstream of *pyrR*)-*Pst*I (in *pyrP*) fragment was subcloned into pUK19, and the resulting pCHA2392 was integrated into the *B. subtilis* chromosome to produce KSS1200 (Fig. 1). Attempts to excise the plasmid containing the entire *ileS* from KSS1200 with various restriction endonucleases failed, suggesting that the expression of *B. subtilis ileS* is lethal to *E. coli* even though low-plasmid-copy-number hosts were used. *B. subtilis* aminoacyl tRNA synthetase genes contain a T-box sequence, a highly conserved regulatory region between the promoter and structural gene which contains a *Kpn*I site (19). Southern blot analysis indicated that there is a *Kpn*I site at a comparable location in *ileS* (8). A 10.3-kb plasmid,

TABLE 2. Plasmids used in this study

Plasmid	Description	Source or reference
pAV2210	*minC* knockout plasmid; Cm^r	39
pCHA2346	12-kb *Eco*RI excision from KSS1180 DNA	This work
pCHA2361	0.85-kb *Eco*RI-*Bgl*II *ileS* insert in pUCAT19	This work
pCHA2392	*Cla*I (5′ to *pyrR*)-*Pst*I (in *pyrP*) in pUK19	This work
pCHA2406	10.3-kb *Kpn*I excision from KSS1200 DNA	This work
pCHA2409	0.45-kb *Kpn*I-*Eco*RI *ileS* promoter region fragment in pUCAT19	This work
pCHA2412	17-kb *Bgl*II excision from KSS1200 DNA	This work
pCHA2421	1.18-kb *Sph*I (in *pyrD*)-*Bgl*II (in *pyrE*) insert in pUK19	This work
pCHA2468	1.12-kb *Eco*RI fragment (3′ *divIVA*–5′ *ileS*) in pUK19	This work
pCHA2469	6-kb *Pst*I excision from KSS1227 DNA; pUK19	This work
pCHA2474	0.67-kb *Eco*RI (in *div*IVA)-*Kpn*I (in *ileS*) in pUCAT19	This work
pCHA2475	1.36-kb *Pst*I (in *orf*)-*Kpn*I (in *ileS*) in pUCAT19	This work
pCHA2479	6-kb *Pst*I excision from KSS1230 DNA; pUK19	This work
pCHA2480	5.4-kb *Hin*dIII excision from KSS1230; pUCAT19	This work
pCHA2516	*Pst*I-*Tth*111I fragment (internal to *orf*) in pUS19	This work
pCHA2542	DivIVA expression plasmid; Cm^r	This work
pCHA2546	0.39-kb *Eco*RI-*Sal*I *divIVA* fragment in pUK19	This work
pCHA2548	*Pst*I-*Tth*111I (internal to *orf*) in pUS19; insert in orientation opposite to that of pCHA2516	This work
pTV21Δ2	Tn*917* replacement vector	44
pTW880	Expression shuttle vector; Cm^r	42
pUCAT19	pUC19 + *cat* at the *Ssp*I site	This work
pUK19	pUC19 + Km^r	W. G. Haldenwang
pUS19	pUC19 + Sp^r	W. G. Haldenwang

pCHA2406, was excised from KSS1200 DNA by utilizing *Kpn*I. The 0.45-kb *Kpn*I-*Eco*RI fragment of *ileS* (Fig. 1) was subcloned in pUCAT19 to produce pCHA2409.

To bypass *ileS* and its associated toxicity problems, DNA sequences leftward of *ileS* were identified in a *B. subtilis* chromosomal partial library. *B. subtilis* 168 DNA was digested with *Eco*RI and then size fractionated on a 10 to 40% sucrose gradient. Aliquots of individual fractions were electrophoresed in a 0.8% agarose gel, transferred to nitrocellulose filters, and probed with pCHA2409. The stron-

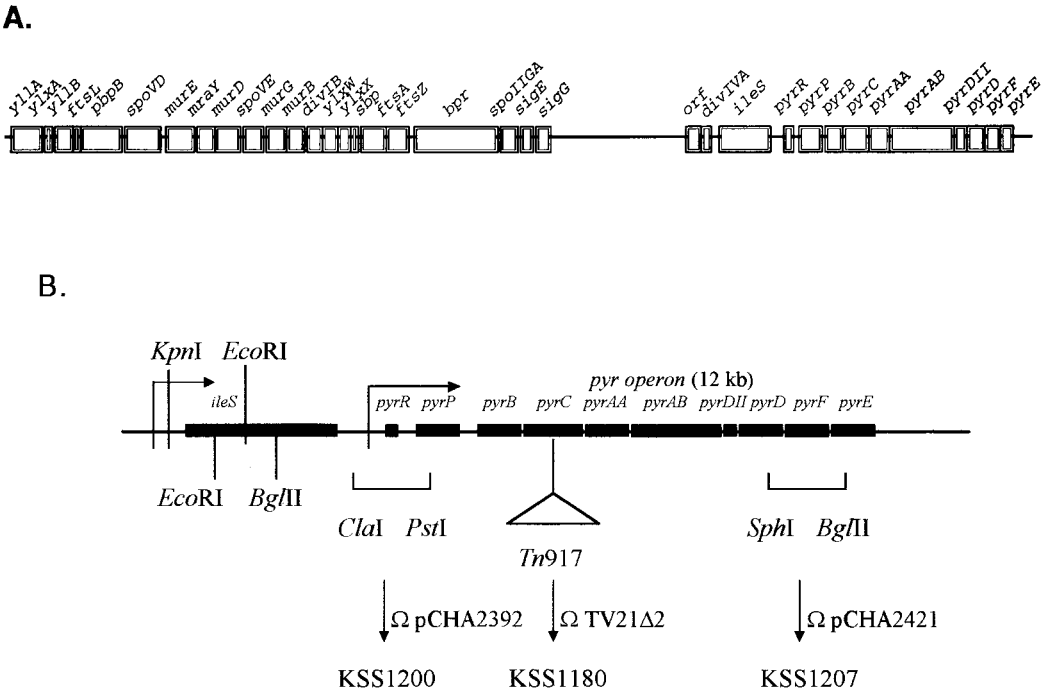

FIG. 1. (A) Genetic organization of the *divIVA* (133°) region of the *B. subtilis* chromosome. The approximately 51-kb sequence contains 35 genes all transcribed colinearly with the direction of replication (left to right as shown). The 28.1-kb sequence extending from *yllA* to *bpr* was assembled from sequences deposited in GenBank. The accession numbers are Z68230 (*yllA-pbpB*); L09703 and Z25865 (*spoVD*); Z15056 and X64258 (*murE*, *mraY*, and *murD*); D14109, X51419, and M15742 (*spoVE*); X64259 and D10602 (*murG*); M31827 and M31800 (*murB*, *divIB*, *ylxW*, and *ylxX*); M22630 and X66239 (*sbp*, *ftsA*, and *ftsZ*); J05400 and M29035 (*bpr*); X17344, M16727, M57606, and X01180 (*spoIIGA* and *sigE*); and J04077 and X57547 (*sigG*). There is an approximately 7-kb gap in the sequence between *sigG* and the sequence presented in this report. The *pyr* operon sequences are from accession number M59757 (31). (B) Physical and genetic organization of the *ileS-pyr* region of the *B. subtilis* chromosome. The Tn*917* insertion site of strain CU4130 is indicated. The restriction fragments which were cloned into the integration vectors are indicated below the genetic map. The plasmids bearing these inserts are indicated to the right of the downward arrows. The strains generated by the integration of these plasmids are indicated below the arrows. The replacement of Tn*917* by the pTV21Δ2 element was as described by Youngman et al. (44). The ORFs are represented by filled boxes. The rightward arrows indicate the promoter sites of the *ileS* determinant and the *pyr* operon.

gest hybridizing fraction was used as insert for ligation into pUK19. The correct clone (pCHA2468) was identified by colony hybridization using the insert of pCHA2409 as probe and confirmed by sequencing both ends of the insert. pCHA2468 was transformed into *B. subtilis* 168, to produce KSS1227. Km^r in KSS1227 was 92% cotransformable with *divIVA*. To isolate additional sequences, a 6-kb plasmid, pCHA2469, whose insert extends from the 5′ *Eco*RI site in *ileS* to the *Pst*I site in *orf* was excised from KSS1227 DNA with *Pst*I. A 5.4-kb plasmid, pCHA2480, whose insert extends from the *Kpn*I site of *ileS* to the *Hin*dIII site, was excised with *Hin*dIII from KSS1232 DNA.

For chromosomal walking in the rightward direction as indicated in Fig. 1, a 17-kb plasmid, pCHA2412, was excised with *Bgl*II from KSS1200 chromosomal DNA. The *Bgl*II-*Sph*I fragment from pCHA2412 was subcloned into pUK19 to produce pCHA2421. This plasmid was integrated into the *B. subtilis* chromosome to produce KSS1207 (Fig. 1).

Genetic linkages. To determine the genetic map positions of the cloned DNA fragments, genetic linkages to *divIVA1* were determined by transforming KSS1168 with chromosomal DNA from KSS1200 or KSS1207 and selecting for kanamycin resistance, and individual colonies were subjected to microscopic screening for the presence of minicells. Also, the genetic linkages to *ftsZ* or *cysC* were also examined with SUIII or JH158, respectively, as recipients. Acquisition of the $ftsZ^+$ or $CysC^+$ markers was determined by growth on tryptic soy agar (TSA) plates at 55°C or by growth on minimal medium plates lacking cysteine, respectively.

Photomicroscopy. Cells were screened for minicells by phase-contrast microscopy. *B. subtilis* cultures for photomicroscopy were grown at 37°C with vigorous aeration to late exponential phase, washed with saline, concentrated in saline to 1/10 of the original volume, and then fixed in 0.5% glutaraldehyde for 15 min on ice. Five microliters of the fixed cells was transferred to slides coated with poly-L-lysine, and phase-contrast micrographs were taken with Kodak TMY-400 film.

Strategy for sequencing the *divIVA1* mutant allele. To sequence the *divIVA1* mutant allele, the 6-kb *Pst*I-generated excision plasmid pCHA2479, cloned as a *Pst*I-generated fragment from KSS1230 DNA, was isolated. This plasmid carries the *divIVA1* allele from KSS1168. The nucleotide sequence of this allele was determined.

Construction of a shuttle expression plasmid containing *divIVA*. To allow for regulated expression of *divIVA* in *B. subtilis*, a shuttle *divIVA* expression plasmid, pCHA2542, was constructed. PCR was utilized to position an *Xba*I site immediately 5′ to the *divIVA* open reading frame (ORF) and an *Sph*I site 3′ to the end of *divIVA*. pCHA2469 served as template, and the primer pair was 5′-TCTAG AATGGAGGTGGCATCATGCC-3′ and 5′-GCATGCATGACTGTCCCTTT CAACCG-3′. The PCR product was cloned in pT7Blue(R) (Novagen). The *Xba*I-*Sph*I PCR product was subcloned into pTW880 (42). The resulting plasmid, pCHA2542, contains *divIVA* under the control of the IPTG (isopropyl-β-D-thiogalactopyranoside)-inducible *spac* promoter.

Sporulation efficiency assay. Sporulation was induced by the nutrient exhaustion method by growth in Schaeffer's liquid sporulation medium (28, 35). After 24 and 48 h of incubation at 35°C, aliquots of the cultures were serially diluted and plated onto TSA both prior to and after a 10-min incubation at 85°C to determine the number of heat-resistant spores present.

Nucleotide sequence accession number. The nucleotide sequence shown in Fig. 3 has been deposited with GenBank under accession number U60901.

RESULTS

Cloning of *divIVA*. From the collection of *B. subtilis* strains bearing genetically mapped inserts of Tn*917* (38), strains with inserts mapping near *divIVA* (144°) were selected. These strains were transformed with pTV21Δ2, thereby replacing the erythromycin resistance of Tn*917* with chloramphenicol resistance (44). The Cm^r gene of KSS1180 (*pyrC*::*21*Δ*2*) was found to be 20% cotransformable with *divIVA*, whereas that of KSS1067 (*zdi-82*::*21*Δ*2*) was only 3% cotransformable with *divIVA*. Thus, *pyrC*::*21*Δ*2* is closer to *divIVA* than *zdi-82*::*21*Δ*2* (map position 140° [37]). Thus, KSS1180 provided the start point for the cloning of *divIVA*. Plasmid clones extending rightward (into the *pyr* operon) and leftward were obtained. These plasmids—pCHA2392, bearing a *Cla*I-*Pst*I fragment leftward from the original Tn*917* insertion site, and pCHA2421, bearing an *Sph*I-*Bgl*II fragment rightward of the Tn*917* insertion site—were introduced into the *B. subtilis* chromosome by single crossover Campbell-like recombination.

The *divIVA1* locus was mapped relative to these plasmid insertions to determine the correct chromosomal walking direction (Fig. 1 and Table 3). Cm^r genes of KSS1200 and KSS1207 were 66 and 11% cotransformable with *divIVA*, respectively. Thus, *divIVA* is located further upstream of the *pyr* operon (leftward in Fig. 1). The genetic linkages to *ftsZ* and *cysC2* were also examined to define the genetic map of this region of the chromosome (Fig. 1 and Table 3). Cm^r genes of KSS1200 and KSS1207 were found to be 24 and 0% cotransformable with *ftsZ*, respectively, suggesting that *ftsZ* is located further upstream from the *pyr* operon, with the implied order being *ftsZ-divIVA-pyr*. Cm^r genes of KSS1200 and KSS1207 were 25 and 68% cotransformable with *cysC*, respectively, suggesting that *cysC* is located downstream from the *pyr* operon. The current genetic map places *divIVA* at 144° with a gene order of *ftsZ-pyr-cysC-divIVA* (30). However, on the basis of these data, the most probable map order is *ftsZ-divIVA-pyr-cysC*. Chromosomal walking and hybridization-based methods were utilized to isolate 7.2 kb of chromosomal DNA upstream of the *pyr* operon.

TABLE 3. Cotransformation frequencies

Donor DNA	Cotransformation frequency (%) with Cm^r or Km^r		
	$divIVA^+$	$cysC^+$	$ftsZ^+$
KSS1200	66	25	24
KSS1180	20	ND[a]	ND
KSS1207	11	68	0

[a] ND, not determined.

Localization of the *divIVA1* mutation. To localize *divIVA*, we used integrational plasmids containing segments of cloned DNA from the 7.2-kb chromosome region to recombinationally correct the *divIVA1* mutation. The *divIVA1* strain KSS1168 was transformed with the integrational plasmids. For correction of the *divIVA1* mutation, the antibiotic-resistant transformants were screened for a wild-type phenotype (absence of minicells and filamentation) by phase-contrast microscopy. Figure 2 shows a physical map of the various plasmid inserts used. $divIVA^+$ correcting activity was obtained with the 1.81-kb *Pst*I-to-*Eco*RI fragment (pCHA2469) (Fig. 2). Removal of the *ileS*-associated sequences had no effect on the correcting activity. Likewise, deletion of the fragment from *Pst*I to the internal *Eco*RI site did not affect $divIVA^+$ restoration. The site of the *divIVA1* mutation was localized to a 390-bp *Eco*RI-*Sal*I fragment upstream of *ileS* (pCHA2546) (Fig. 2).

Nucleotide sequence analysis of the *divIVA* region. Figure 3 shows the nucleotide sequence of a 2.37-kb region extending from the *Hin*dIII site to an *Eco*RI site at the 5′ end of *ileS*. Two complete and one partial ORFs were identified in the sequence. The first, designated *orf*, encodes a protein of 226 amino acids with a molecular weight of 29,069.

The second ORF begins 97 bp downstream of *orf* and consists of 164 codons which can encode a protein of 19,490 Da. This ORF spans the *Sal*I-*Eco*RI fragment bearing *divIVA1* identified in the allele correction study. Therefore, this ORF is *divIVA*. Hydropathy analysis of the DivIVA protein suggests that it is a cytoplasmic protein. Comparison of the amino acid sequence of DivIVA to GenBank sequences revealed sequence similarity to three proteins (2). These include similarity to an ORF of unknown function from *Staphylococcus aureus* (41% identity and 72% similarity over a 158-amino-acid stretch) (18). Interestingly, this staphylococcal ORF is also immediately upstream of *ileS*. DivIVA displays sequence similarity to the antigen 84 (Ag 84) proteins of *Mycobacterium tuberculosis* and *Mycobacterium leprae*. DivIVA is 34.4 and 31.9% identical and 60.8 and 57.2% similar to the Ag 84 proteins, respectively (with windows of 125 and 138 residues [20]). The function(s) of the Ag 84 proteins is unknown. The *M. tuberculosis* protein was

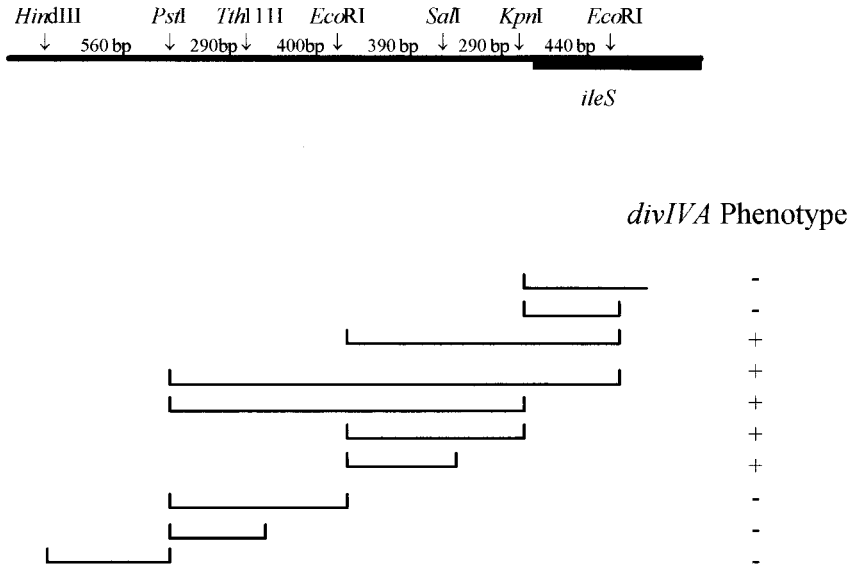

FIG. 2. *divIVA1* recombinational correction analysis. Integrational plasmids were constructed with inserts shown below the physical map of the *ileS* upstream region. The plasmids were introduced into KSS1168 (*divIVA1*), and the antibiotic-resistant transformants were examined by phase-contrast microscopy for a minicell phenotype. +, the plasmid corrects the *divIVA1* mutation, resulting in a wild-type phenotype; −, the plasmid failed to correct *divIVA1*, resulting in retention of the minicell phenotype. The insert of pCHA2406 is a 6.1-kb fragment extending to a *Pst*I site in *pyrP* (Fig. 1).

found to be cytoplasmic (20). The *S. aureus ileS* upstream ORF does not show a correspondingly high similarity with the mycobacterial Ag 84 proteins.

The third partial ORF is *ileS*. The order of genes in the *divIVA* region of the *B. subtilis* chromosome is *orf-divIVA-ileS-pyrR-pyrP-pyrB-pyrC-pyrAA-pyrAB-pyrDII-pyrD-pyrF-pyrE*, with all of these genes being transcribed from left to right, in the same direction as the movement of the replication fork (Fig. 1A).

Sequence of the *divIVA1* allele. To identify the mutational change in the *divIVA1* allele, the entire *divIVA* loci of both *B. subtilis* 168 and KSS1168 were sequenced and compared. The excision plasmids bearing the *divIVA* alleles were characterized for biological activity. The *divIVA1* allele could be introduced into *B. subtilis* 168 by transformation with pCHA2479, whereas the *divIVA1* allele of KSS1168 could be corrected by transformation with pCHA2469. The entire *divIVA1* ORF from pCHA2479 was sequenced. Only a single mutational alteration was identified. The *divIVA1* allele contains a G-to-A transition at nucleotide position 232 in the *divIVA* ORF (nucleotide position 1404 in Fig. 3) resulting in an alanine-to-threonine substitution at amino acid residue 78.

Inactivation of *divIVA* results in a minicell phenotype. To determine the role of *divIVA*, inactivation of the determinant was carried out. The *divIVA* ORF was disrupted by the insertion of a *cat* or Pm^r cassette at the *Eco*RI site (Fig. 4A). The correct positioning of these cassettes within the *divIVA* determinant was verified by Southern blot hybridization (8). The resulting DivIVA$^-$ strains, KSS1237 and KSS1254, exhibit a minicell phenotype similar to that of KSS1168 (Fig. 5B to D). The isolation of viable DivIVA$^-$ mutants indicates that *divIVA* is not an essential gene of *B. subtilis.*

A *cat* cassette was also inserted at the *Sal*I site at the 3′ end of *divIVA*, seven codons from the 3′ terminus. Insertion of the *cat* cassette at this position results in a change in the C-terminal sequence from seven residues (VDAVFEEKE) to eight different residues (VDLQVSGVVI). The resulting strain, KSS1248, displayed a wild-type phenotype, indicating that the seven C-terminal amino acids are not necessary for DivIVA function (Fig. 5E). This result explains why a wild-type phenotype was obtained when the plasmid bearing the *Eco*RI-*Sal*I fragment wholly internal to *divIVA* (pCHA2546) was integrated into the *B. subtilis* chromosome (Fig. 2). A functional truncated product was produced rather than an inactive truncated gene product.

The phenotype of the DivIVA$^-$ mutants differs from that of a DivIVB$^-$ mutant (compare Fig. 5B to D with 5F). The latter strain is less filamentous and produces minicells at a greater frequency. To determine the phenotype of a DivIVA$^-$ DivIVB$^-$ double mutant, the *divIVA*::Pm^r determinant was introduced into strain KSS1178 (*minC*::pAV2210) by transformation. The double mutant displays a minicell phenotype identical to that of the MinC$^-$ mutant, indicating that the DivIVB$^-$ phenotype is dominant to the DivIVA$^-$ phenotype (Fig. 5G).

Inactivation of the *divIVA* upstream ORF. Plasmid pCHA2516 or pCHA2548 containing *Pst*I-*Tth111I* chromosomal fragments wholly internal to *orf* was integrated into the chromosome of *B. subtilis* 168, resulting in insertional inactivation of this ORF (Fig. 4B). The two plasmids have the same chromosomal insert in pUS19 but in opposite orientations. Through the use of this plasmid pair, two questions were addressed. The first was what is the phenotype of *orf*-inactivated *B. subtilis*. The second question was whether there is a promoter between *orf* and *divIVA*. If *orf* and *divIVA* are coexpressed, the inactivation of *orf* would likely cause a polar effect on *divIVA* expression and should result in a minicell phenotype. If *orf* and *divIVA* are transcribed independently, no polar effects on *divIVA* would be observed. Integration of either pCHA2516 or pCHA2548 resulted in no observable alteration in cell division (Fig. 5H). No minicell formation was observed, suggesting no polar effects on *divIVA*. Use of plasmids with oppositely oriented inserts results in integration of the pUS19 vector in opposite orientations in the *B. subtilis* chromosome (Fig. 4B). Thus, it is unlikely that expression of *divIVA* would result from a vector promoter. These results suggest that *divIVA* is expressed independently of *orf*, and the two proteins appear to be functionally unrelated.

Overexpression of DivIVA in *B. subtilis*. To determine the phenotype produced when DivIVA is overexpressed in *B. sub-*

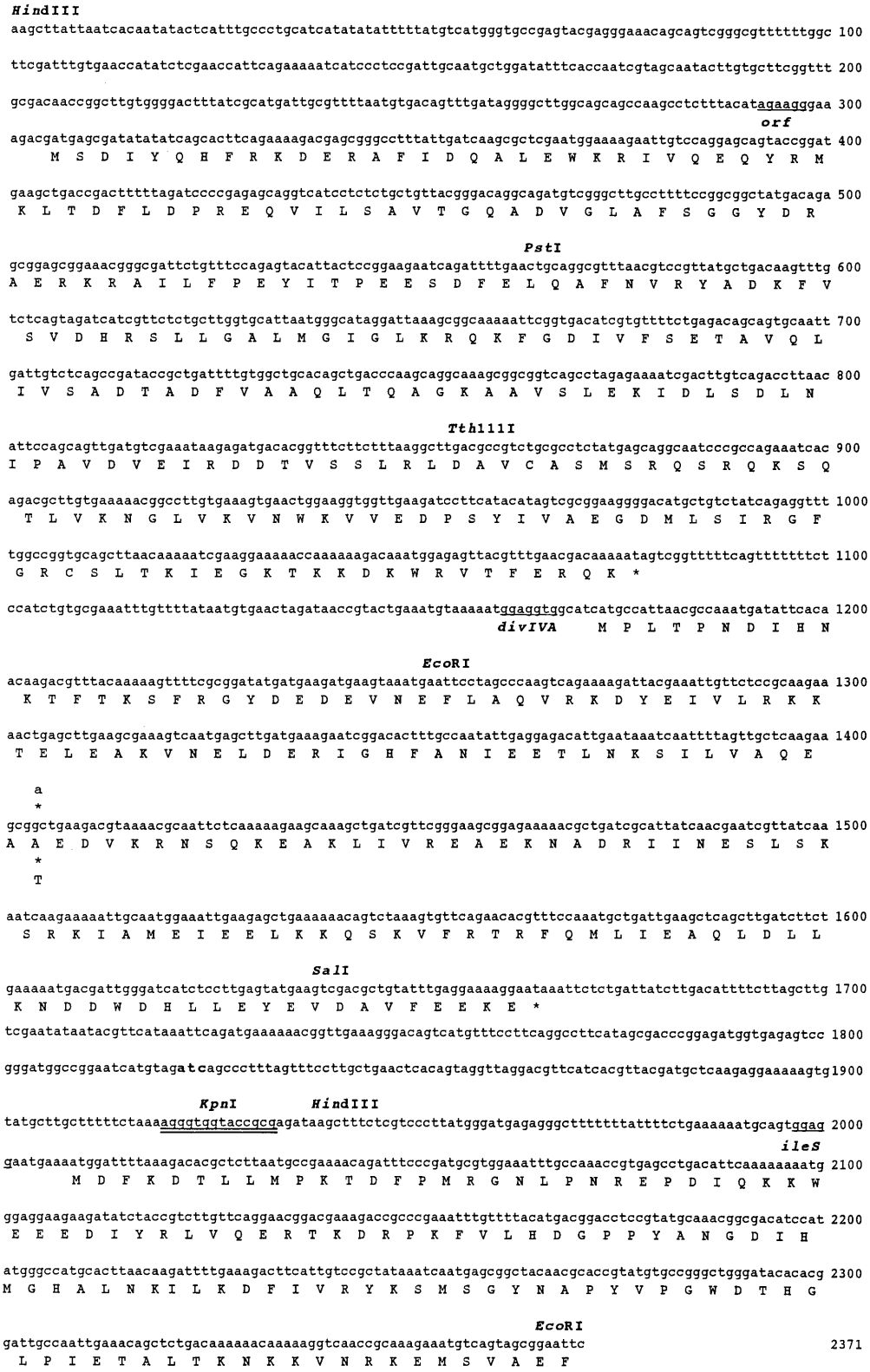

FIG. 3. Nucleotide sequence of the nontranscribed strand of the *divIVA* region. The translated polypeptide is shown below the nucleotide sequence, with the one-letter designation of each amino acid residue positioned below the first nucleotide of the codon. Putative ribosome binding sites are underlined. The gene names are given below the ribosome binding sites. The T-box sequence of *ileS* is doubly underlined. The guanine-to-adenine transition of the *divIVA1* allele resulting in an alanine-to-threonine substitution is indicated by the asterisks at position 1404. Landmark restriction endonuclease recognition sites are indicated above the nucleotide sequence.

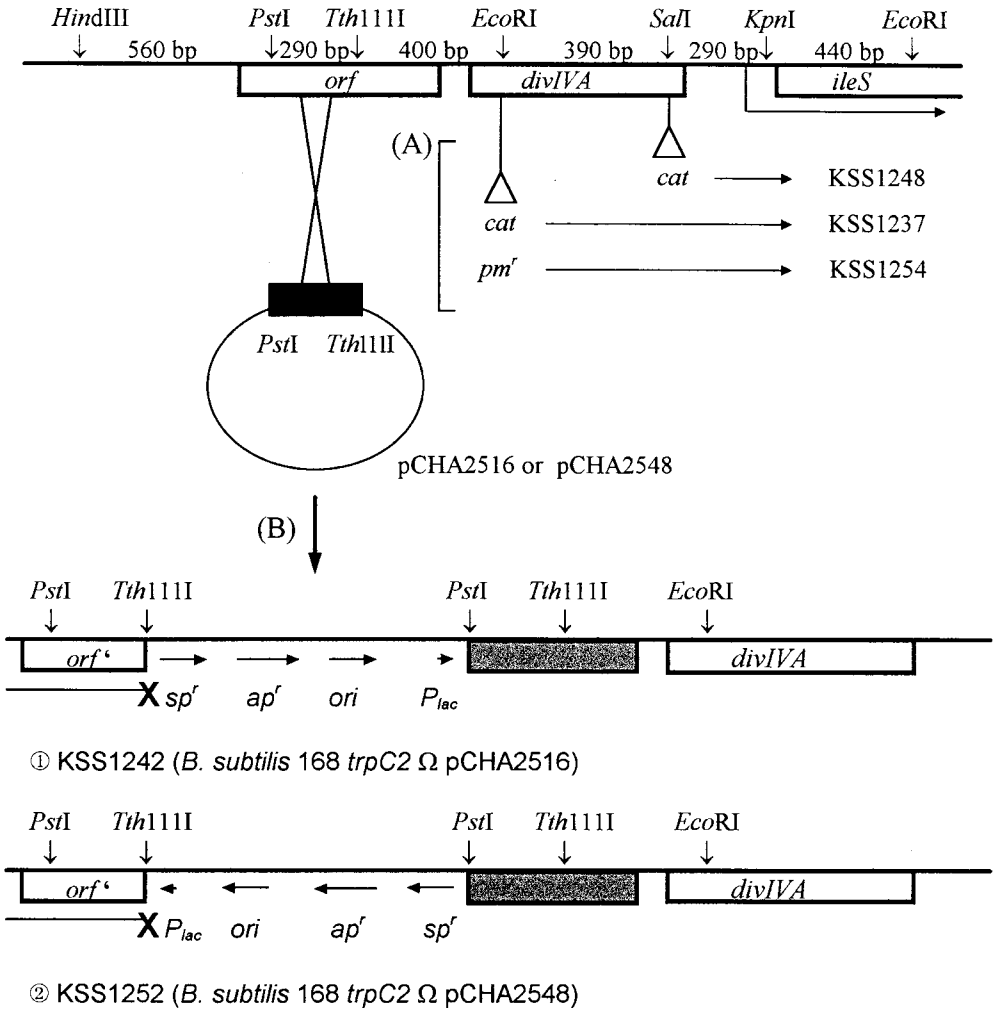

FIG. 4. Insertional inactivation of *divIVA* and *orf*. A physical map of the *divIVA* region of the *B. subtilis* chromosome is shown at the top of the figure, with the ORFs represented by boxes. (A) The *divIVA* determinant was insertionally inactivated at its *Eco*RI site with a chloramphenicol acetyltransferase cassette (to generate strain KSS1237) or a phleomycin resistance cassette (36) (to generate strain KSS1254). Insertion of the *cat* cassette at the *Sal*I site at the 3′ end of the ORF produced strain KSS1248. (B) Insertional inactivation of *orf* was accomplished by the integration of pCHA2516 or pCHA2548. These plasmids carry the *Pst*I-*Tth*111I fragment (filled box) wholly internal to *orf* but in the opposite orientation. Integration of these plasmids results in the DNA arrangements shown in panel B. The plasmid insertions result in inactivation of *orf* (×). The *orf*′ box and shaded box are 5′-end and 3′-end truncated ORFs, respectively. Abbreviations: ap^r, ampicillin resistance determinant; cat, chloramphenicol acetyltransferase cassette; ori, plasmid replication functions; P_{lac}, promoter for the vector *E. coli lacZ*α peptide determinant; pm^r, phleomycin resistance cassette; sp^r, spectinomycin resistance determinant.

tilis, the *divIVA* ORF was cloned under the control of the IPTG-inducible *spac* promoter in pTW880 (42). The resulting plasmid, pCHA2542 (Fig. 6A), was introduced into *B. subtilis* 168. The transformants displayed two types of colony morphology despite the lack of IPTG induction (Fig. 6B). A small, compact colony type and a large, spreading (wild-type) colony type were obtained. During subculture of the small colony type, the large colony type appeared and overgrew the small colony type. Phase-contrast microscopic examination indicated the *B. subtilis* cells in the small colony type were very filamentous but the cells from the large colony type were normal in cellular morphology. Residual *divIVA* expression from the leaky *spac* vector appeared to be division inhibitory to *B. subtilis*. Mutations which negate this inhibition of division would give rise to the large-colony segregants. To determine the genetic location of the secondary mutation, plasmids were isolated from cells comprising the small and large colony types and were introduced in *B. subtilis* 168. The plasmid from the small-colony transformants gave the unstable small colony phenotype, but the plasmids from the large colony type gave rise only to large colony transformants, suggesting that the secondary mutation occurred in the plasmid DNA. Physical mapping of the plasmids indicated that the plasmid from the large colony type contained large deletions which included the 5′ end of the *divIVA* ORF. Therefore, no DivIVA was synthesized from the plasmid. The plasmid from the small-colony-type cells also contained a small deletion, but at the 3′ end of *divIVA*. The plasmid from the small colony type would direct the synthesis of a truncated DivIVA which was still functional as an inhibitor of cell division.

It appeared, therefore, that DivIVA expression is tolerated only at very low levels. To reduce the lethal effect of *divIVA* overexpression in *B. subtilis*, the DivIVA expression plasmid was introduced in KSS1254, which lacks a functional copy of *divIVA*. The resulting transformant, KSS1258, gave rise to a single colony type whose cells were only moderately filamentous (Fig. 7C). Physical mapping of the plasmid isolated from KSS1258 indicated that the plasmid was structurally intact. The

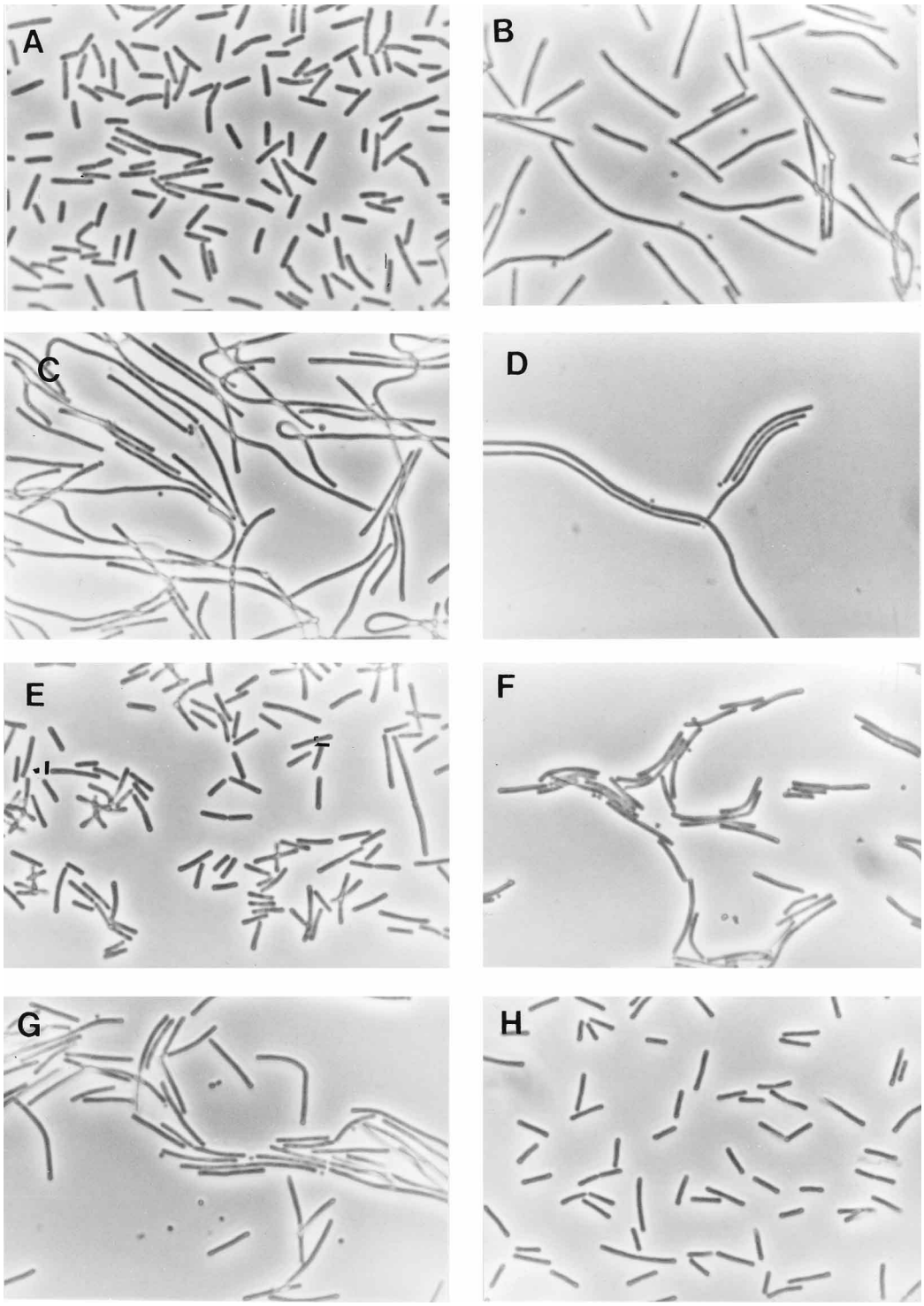

FIG. 5. Phase-contrast micrographs showing minicell phenotypes. (A) KSS1001, wild type; (B) KSS1168, *divIVA1*; (C) KSS1237, *divIVA*::*cat*; (D) KSS1254, *divIVA*::Pm^r; (E) KSS1248, *divIVA*::*cat* (at the *Sal*I site); (F) KSS1178, *minC*::pAV2210; (G) KSS1263, *divIVA*::Pm^r *minC*::pAV2210; (H) KSS1252, *orf*::pCHA2548. Magnification, ×1,160.

induction of *divIVA* expression in KSS1258 by the addition of IPTG (to 2 mM) resulted in an extensively filamentous phenotype (Fig. 7D). Introduction of pCHA2542 into the *divIVA1* mutant produced KSS1266. In the absence of IPTG induction, KSS1266 exhibited a phenotype similar to that of its parent strain, KSS1168 (Fig. 7G). With the addition of IPTG to 2 mM, the moderately filamentous phenotype disappeared, although minicell formation remained evident (Fig. 7H). Thus, the introduction of pCHA2542 into a strain lacking DivIVA (KSS1258) resulted in a filamentous, but non-minicell-forming,

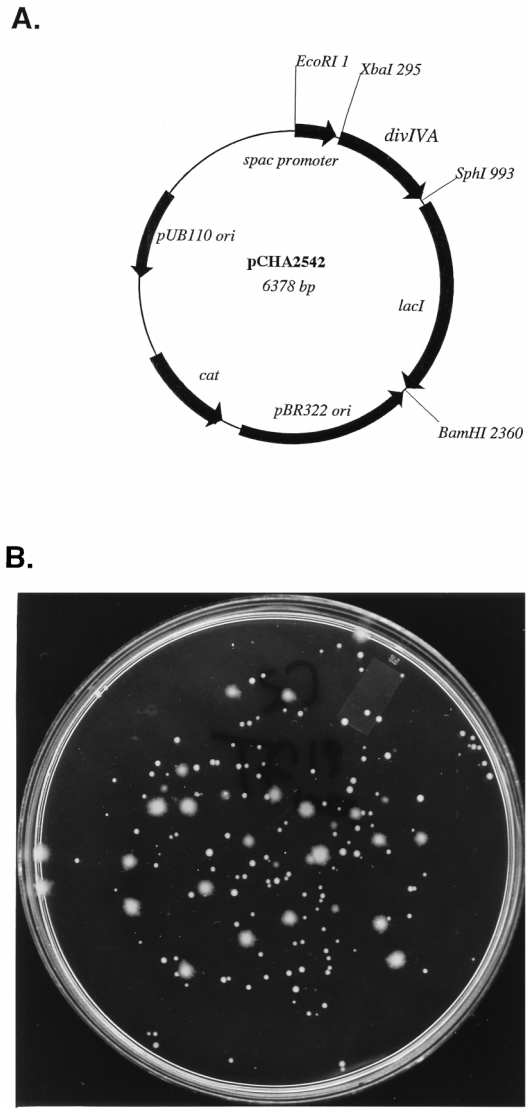

FIG. 6. (A) DivIVA expression plasmid pCHA2542. The *divIVA* ORF with its native ribosome binding site was cloned downstream of an IPTG-inducible *spac* promoter. The plasmid is a shuttle vector, able to replicate in either *E. coli* or *B. subtilis*. (B) Large and small colony types arising from introduction of pCHA2542 into KSS1001. The transformed cells were plated onto TSA containing 5 μg of chloramphenicol per ml but without IPTG. The plate was incubated for 24 h at 37°C.

phenotype, while the same plasmid in the *divIVA1* point mutant strain produced less filamentation and there was incomplete complementation of the minicell-forming phenotype. It would appear that the defective DivIVA1 protein may compete with the wild-type plasmid-encoded protein. Thus, higher expression levels may be necessary to achieve the same degree of minicell complementation and division inhibition. This postulated competition may also explain sporulation results obtained with the two *divIVA* mutant strains (see below).

To determine if the presence of pCHA2542 would result in a filamentous phenotype in the absence of a functional MinCD system, the plasmid was transformed into strain KSS1101 to produce strain KSS1264. Despite the presence of a wild-type *divIVA* gene in this strain's chromosome, the plasmid was stably maintained. The plasmid-bearing cells, with or without IPTG induction, were no more filamentous than the control culture lacking the plasmid insert (Fig. 7E and F). Thus, *divIVA* appears to require the MinCD proteins in order to inhibit septation and produce filamentous growth.

A role for DivIVA in sporulation. During the process of endospore formation, an asymmetric septation event occurs which results in the establishment of the forespore and mother cell compartments. Therefore, it was of interest to determine whether DivIVA functions in this polar septation event. Various *B. subtilis* mutants were examined for sporulation efficiency, and the results are presented in Table 4. The *divIVA1* mutant gave a greater than 10^4-fold reduction in endospore production. However, when KSS1254 bearing the insertionally inactivated *divIVA* was examined, its reduction in sporulation frequency was more modest, only about fivefold. When Schaeffer's broth cultures were allowed to incubate an additional 24 h prior to sampling (48 h total), the sporulation frequency of the KSS1168 point mutant had improved to be more similar to that of the insertionally inactivated *divIVA* strain KSS1254. The former gave 30-fold reduction in sporulation efficiency. The *divIVB1* mutant sporulated with an approximately normal frequency in agreement with previous findings (26). However, viable counts and spore counts were consistently about 10-fold lower than those of the wild-type strain in the sporulation medium. Sporulation efficiencies in the DivIVA$^-$ and DivIVB$^-$ double-mutant strains were examined. Strain KSS1261 (*divIVA1* DivIVB$^-$) exhibited the same sporulation efficiency as the *divIVA1* *divIVB*$^+$ strain (KSS1168), while KSS1263 (*divIVA*::Pm^r DivIVB$^-$) exhibited the same sporulation efficiency as the *divIVA*::Pm^r *divIVB*$^+$ strain (KSS1254). Thus, *divIVA* is dominant to *divIVB* with regard to sporulation effects. Inactivation of *orf* had no effect on sporulation frequency.

The *divIVA* point mutant and the insertionally inactivated mutant exhibited markedly different sporulation efficiencies at the 24-h time point even though their vegetative growth phenotypes were similar. To determine whether an additional factor(s) was responsible for this difference, insertional inactivation of the *divIVA1* allele was carried out. The resulting mutant (KSS1262 *divIVA1*::Pm^r) exhibited the same sporulation efficiency as that observed with the insertional inactivation of the wild-type allele. Therefore, the sporulation defect arising from the DivIVA protein with the alanine-to-threonine substitution is more severe than that arising from the complete loss of the DivIVA protein.

DISCUSSION

The DivIVA$^-$ strains display a minicell and moderately filamentous phenotype. The DivIVA$^-$ phenotype differs from the DivIVB$^-$ phenotype. The DivIVB$^-$ strains produce spherical minicells (as well as short rods of varying length) at greater frequency than the DivIVA$^-$ strains, whereas the DivIVA$^-$ strains produce fewer minicells (all spherical) and exhibit more extensive filamentation. Interestingly, the phenotype of the double mutants (DivIVA$^-$ DivIVB$^-$) is identical to that of the DivIVB$^-$ mutant, indicating that *divIVB* is epistatic to *divIVA*. In the absence of the DivIVB proteins (MinCD), loss of DivIVA function provides no further impediment to the division process. Furthermore, the septation inhibitory effect of DivIVA overproduction is not present in the DivIVB$^-$ mutants. The fact that DivIVA appears to require the presence of the MinCD proteins for activity suggests that the DivIVA protein may function via the MinCD proteins.

Because an asymmetric septation event is utilized to establish the forespore and mother cell compartments during the sporulation process, it was of interest to determine whether the

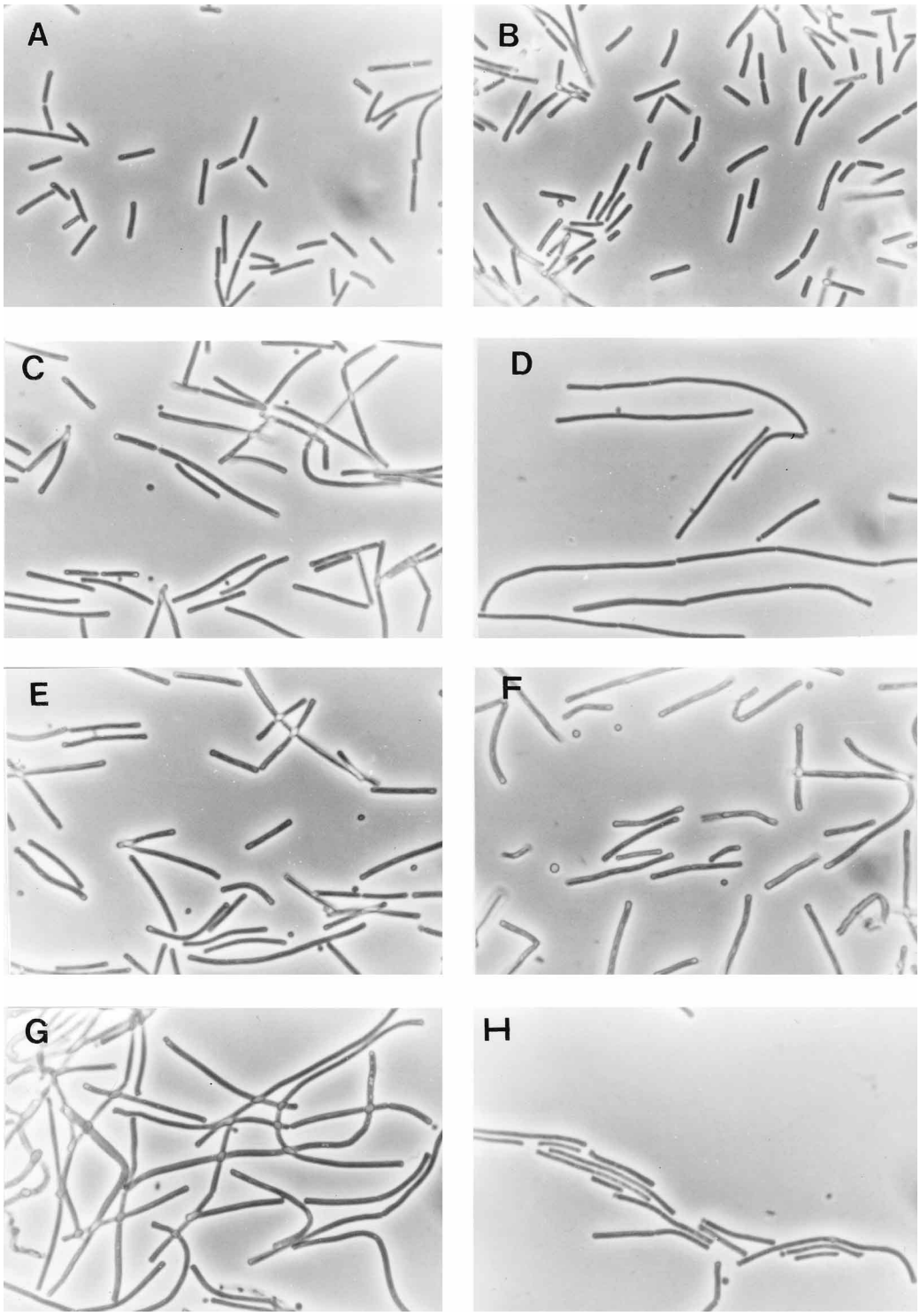

FIG. 7. Phase-contrast micrographs showing the effects of IPTG induction of DivIVA production in various *B. subtilis* mutants. The cells were grown in tryptic soy broth containing 5 μg of chloramphenicol per ml to early log phase (A_{500}, 0.3). IPTG was then added to a final concentration of 2 mM. A control culture was included which lacked IPTG. Incubation of the cultures continued until A_{500} was 0.8. (A) KSS1182 (pTW880 vector control); (B) KSS1182 with induction; (C) KSS1258 (*divIVA*::Pm^r, pCHA2542); (D) KSS1258 with induction; (E) KSS1264 (*divIVB1*, pCHA2542); (F) KSS1264 with induction; (G) KSS1266 (*divIVA1*, pCHA2542); (H) KSS1266 with induction. Magnification, ×1,160.

DivIVA or DivIVB protein plays a role in the sporulation. We found, as did Levin et al. (26), that DivIVB$^-$ mutants sporulate at approximately a wild-type-level frequency. The slight reduction in frequency that we observed at 24 h is similar to the modest reduction in sporulation efficiency at 24 h reported by Lee and Price (23). In contrast, *divIVA* mutants showed a more pronounced defect in sporulation. However, the sporulation frequencies improved with these mutants if the incubation

TABLE 4. Sporulation efficiencies

Strain	Spore titer (relative efficiency[a])	
	24 h	48 h
KSS1001 (wild type)	3.1×10^8 (1)	5.1×10^8 (1)
KSS1168 *divIVA1*	6.5×10^3 (7.4×10^{-5})	1.7×10^7 (0.03)
KSS1178 *divIVB1*	3.2×10^7 (0.8)	7.0×10^7 (1)
KSS1254 *divIVA*::Pm^r	1.5×10^7 (0.2)	5.3×10^7 (0.4)
KSS1248 *divIVA*::*cat* (*Sal*I)	1.6×10^8 (0.8)	ND[b]
KSS1252 *orf*::pCHA2548	2.5×10^8 (1)	ND
KSS1263 *divIVA*::Pm *divIVB1*	7.8×10^6 (0.2)	3.3×10^7 (0.4)

[a] Defined as (CFU of spores/total viable CFU)/(viable KSS1001 spores/KSS1001 total viable CFU).
[b] ND, not determined.

period was continued to 48 h. This implies that the loss of DivIVA function results in a delay in the sporulation process rather than a complete block.

Because the DivIVA protein appears to function through MinCD, it was possible that the sporulation defect of DivIVA$^-$ strains would be lost in a DivIVB$^-$ background. To address this question, the sporulation efficiencies of the DivIVA$^-$ DivIVB$^-$ double mutants were examined. Because the DivIVA$^-$-associated sporulation defects were not corrected in the DivIVB$^-$ background, the sporulation-associated function of DivIVA appears to be independent of MinCD.

The question remains as to whether *divIVA* is the *minE* homolog of *B. subtilis*. The evidence that point mutations or insertion mutations in the *B. subtilis minC* or *minD* genes lead to a minicell phenotype indicates the functional similarity of the *B. subtilis* and *E. coli* Min proteins. The only evidence to date which may be at odds with this view is the observation that, when the *minCD* genes were introduced into *B. subtilis* on a plasmid vector, a minicell phenotype resulted rather than the predicted filamentation (26, 39). However, the *minCD* subcloning was accomplished with the restriction endonuclease *Bgl*II, which cleaves at the termination codon of *minD*. Thus, the plasmid clones would express a *minD-lacZ*α fusion protein with additional C-terminal residues, and the fusion product may not be fully functional (26, 39). Elevated levels of the nonfunctional MinD protein may outcompete the wild-type MinD protein present in the cell and thus cause the observed minicell formation.

Thus far, no *B. subtilis* counterpart of the *E. coli minE* determinant has been identified. Rothfield and Zhao proposed that the *divIVA* locus might be the site of the missing *minE* determinant (33). The *divIVA* protein does not, however, have properties consistent with it performing the exact function of *minE*. First of all, the amino acid sequences of the DivIVA and MinE proteins do not exhibit any significant similarity. If *divIVA* were to function exactly as *minE*, inactivation of *divIVA* should result in a filamentous phenotype whereas overexpression would generate a minicell phenotype. The opposite results were obtained. Therefore, *divIVA* cannot function in a manner identical to the *E. coli* MinE protein. However, DivIVA does appear to perform the same function as MinE but by a different mechanism. A functional interaction between DivIVA and MinCD is supported by the phenotype of the double-mutant strains and the lack of septation inhibition when *divIVA* was introduced on an expression plasmid into the DivIVB$^-$ mutant.

To explain the roles of DivIVA in the division process during vegetative growth and sporulation in *B. subtilis*, a model is proposed based on the results of this study (Fig. 8). The DivIVA

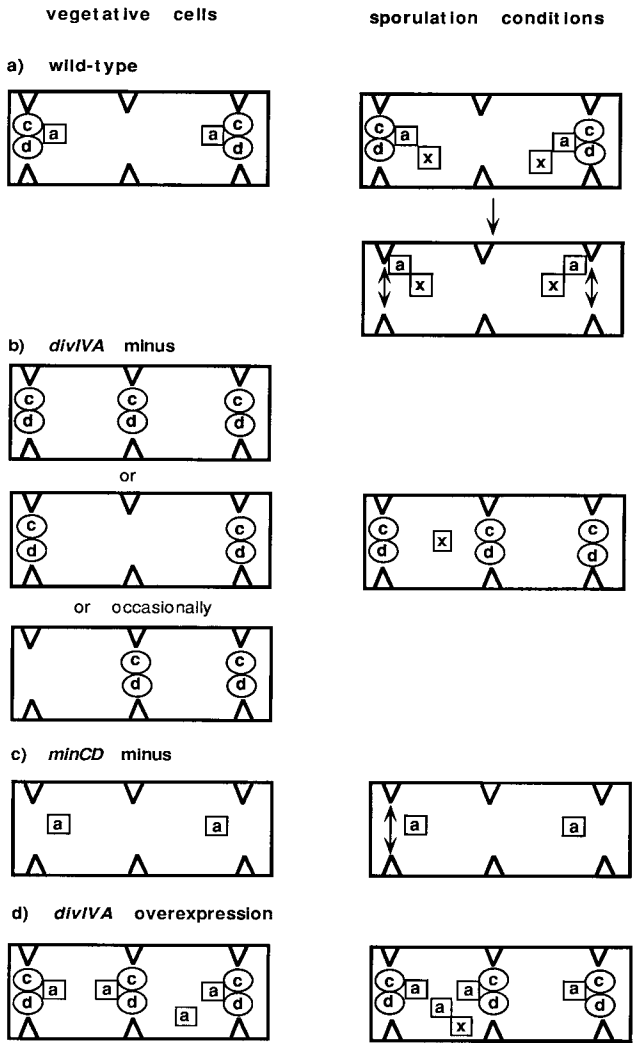

FIG. 8. Proposed model of DivIVA action. Diagrammatic representation of a model that describes the proposed role of the *divIVA* gene product during vegetative growth and during sporulation of *B. subtilis*. Circles c and d, MinC and MinD proteins encoded by the *divIVB* operon. The DivIVA protein is represented by box a. Box x, hypothetical sporulation-associated protein. The three potential septation sites are indicated. See the text for details.

protein is proposed to have an affinity for the polar septation sites. During vegetative growth of wild-type *B. subtilis*, the DivIVA protein may function as a pilot protein to direct MinCD to the polar septation sites to inhibit cell division at these inappropriate sites (Fig. 8a). The DivIVA protein is envisioned to have a lower affinity for the midcell septation site, and thus, at physiological levels of this protein, inhibition does not occur at midcell. In a DivIVA$^-$ mutant, there is no pilot protein to direct MinCD to the polar sites so that the polar sites are occasionally utilized (Fig. 8b). Therefore, the DivIVA$^-$ mutant produces minicells. The DivIVA$^-$ cells are also very filamentous. The filamentation phenotype would be the consequence of two events. First, a moderate filamentation, like that observed with DivIVB$^-$ mutants, would result from the minicell divisions. A second cause of filamentation would be that, without the pilot protein to direct MinCD to the polar sites, MinCD would be available to block septation at midcell, thus giving rise to filamentous growth. The polar and midcell inhibitions are somewhat leaky, giving rise to some

minicells and some residual cell division. The latter explains why the *divIVA* mutations are not lethal. In a MinCD$^-$ strain, there is no septation repressor with which the DivIVA pilot protein can interact. Because DivIVA has no septation-inhibitory properties without MinCD, all septation sites are available and minicell formation results (Fig. 8c). Elevated concentrations of DivIVA direct MinCD to the primary polar sites as well as the secondary central site, resulting in inhibition at all these sites thus inducing the extensive filamentation (Fig. 8d). According to the model, DivIVA$^-$ MinCD$^-$ double mutants should exhibit the same phenotype as the MinCD$^-$ mutant, and this was experimentally shown to be the case.

Under sporulation conditions, an unknown sporulation factor, designated x, is postulated to interact with DivIVA to make available the polar septation sites for the sporulation-associated septation event (Fig. 8a). The observation that the FtsZ ring forms initially at both polar sites suggests that MinCD inhibition of FtsZ assembly at both polar septation sites is prevented early in the sporulation process (25). It is not yet known why septation at one of the polar sites is subsequently inhibited. In DivIVA$^-$ strains, there would be no DivIVA to direct factor x to the polar sites. Factor x localization to the polar site would thus become inefficient, resulting in a pronounced delay in sporulation (Fig. 8b). The *divIVA1* mutant exhibits remarkably decreased sporulation efficiency compared to strains in which *divIVA* is insertionally inactivated. The mutated DivIVA1 protein could possibly interact with (absorb) factor x but be defective in polar site localization. The reduction in the availability of free factor x to bind, albeit inefficiently, to the polar site or a reduced efficiency of the DivIVA1-x complex to so bind would result in a greater delay in sporulation than would be found if DivIVA was totally absent (Fig. 8c). The observation that MinCD$^-$ mutants more efficiently sporulate than do DivIVA$^-$ mutants suggests that DivIVA can bind to the polar sites and to factor x without first interacting with MinCD. Because factor x interacts with DivIVA and not MinCD, the DivIVA$^-$ DivIVB$^-$ mutants should behave the same as DivIVA$^-$ strains with regard to sporulation. This was found to be the case.

A test of this model will require an examination of interactions between the MinCD septation inhibitor and DivIVA. Antibodies to DivIVA and MinC are being generated for this purpose.

Many questions still remain to be answered. If MinCD is the only septation repressor, mutants resulting in loss of MinCD function should produce 67% minicells with only 33% of the divisions occurring at midcell. However, minicell frequencies are only on the order of 31% or less for *minC* or *minD* mutants (8, 9). Therefore, other systems are likely to be present which regulate septation site selection. The molecular details of this process will not be fully understood until the chemical nature of a potential septation site is determined. Until this occurs, genetic studies of the cell division process will continue to be the most productive path to gain insight into the process of binary fission by bacteria.

ACKNOWLEDGMENTS

We thank John Reeve (Ohio State University) for providing the *divIVA1* derivative of strain CU403, R. G. Wake (University of Sydney) for strain SUIII, and Duane Kerr for help with the photography.

This work was supported by Public Health Service grant GM37990 from the National Institutes of Health.

REFERENCES

1. **Adler, H. I., W. D. Fisher, A. Cohen, and A. H. Hardigree.** 1967. Miniature *Escherichia coli* cells deficient in DNA. Proc. Natl. Acad. Sci. USA **57:**321–326.
2. **Altschul, S. F., W. Gish, W. Miller, E. W. Myers, and D. J. Lipman.** 1990. Basic local alignment search tool. J. Mol. Biol. **215:**403–410.
3. **Beall, B., and J. Lutkenhaus.** 1991. FtsZ in *Bacillus subtilis* is required for vegetative septation and for asymmetric septation during sporulation. Genes Dev. **5:**447–455.
4. **Beall, B., and J. Lutkenhaus.** 1992. Impaired cell division and sporulation of a *Bacillus subtilis* strain with the *ftsA* gene deleted. J. Bacteriol. **174:**2398–2403.
5. **Bi, E., and J. Lutkenhaus.** 1990. Interaction between the *min* locus and *ftsZ*. J. Bacteriol. **172:**5610–5616.
6. **Birnboim, H. C., and J. Doly.** 1979. A rapid alkaline extraction procedure for screening recombinant plasmid DNA. Nucleic Acids Res. **7:**1513–1523.
7. **Butler, Y. X., Y. Abhayawardhane, and G. C. Stewart.** 1993. Amplification of the *Bacillus subtilis maf* gene results in arrested septum formation. J. Bacteriol. **175:**3139–3145.
8. **Cha, J.-H., and G. C. Stewart.** 1996. Unpublished data.
9. **Coyne, S. I., and N. H. Mendelson.** 1974. Clonal analysis of cell division in the *Bacillus subtilis divIV-B1* minicell-producing mutant. J. Bacteriol. **118:**15–20.
10. **Dagert, M., and S. D. Ehrlich.** 1979. Prolonged incubation in calcium chloride improves the competence of *Escherichia coli* cells. Gene **6:**23–28.
11. **de Boer, P. A. J., R. E. Crossley, A. R. Hand, and L. I. Rothfield.** 1991. The MinD protein is a membrane ATPase required for the correct placement of the *Escherichia coli* division site. EMBO J. **10:**4371–4380.
12. **de Boer, P. A. J., R. E. Crossley, and L. I. Rothfield.** 1989. A division inhibitor and a topological specificity factor coded for by the minicell locus determine the proper placement of the division septum in *E. coli*. Cell **56:**641–649.
13. **de Boer, P. A. J., R. E. Crossley, and L. I. Rothfield.** 1990. Central role for the *Escherichia coli minC* gene product in two different division inhibition systems. Proc. Natl. Acad. Sci. USA **87:**1129–1133.
14. **de Boer, P. A. J., R. E. Crossley, and L. I. Rothfield.** 1992. Roles of MinC and MinD in the site specific septation block mediated by the MinCDE system of *Escherichia coli*. J. Bacteriol. **174:**63–70.
15. **Doi, M., M. Wachi, F. Ishino, S. Tomioka, M. Ito, Y. Sakagami, A. Suzuki, and M. Matsuhashi.** 1988. Determinations of the DNA sequence of the *mreB* gene and of the gene products of the *mre* region that function in formation of the rod shape of *Escherichia coli* cells. J. Bacteriol. **170:**4619–4624.
16. **Erickson, R. J., and J. C. Copeland.** 1972. Structure and replication of chromosomes in competent cells of *Bacillus subtilis*. J. Bacteriol. **109:**1075–1084.
17. **Feinberg, A. P., and B. Vogelstein.** 1984. Addendum: a technique for radiolabeling DNA restriction endonuclease fragments to high specific activity. Anal. Biochem. **137:**266–267.
18. **Grundy, F. J., G. M. Hornblow, J. M. Ward, A. F. Chalker, and T. M. Henkin.** 1996. The Staphylococcus aureus *ileS* gene, encoding isoleucyl-tRNA synthetase, is a member of the T box family. GenBank accession number U41072.
19. **Grundy, F. J., and T. M. Henkin.** 1994. Conservation of a transcription antitermination mechanism in aminoacyl-tRNA synthetase and amino acid biosynthesis genes in gram-positive bacteria. J. Mol. Biol. **235:**798–804.
20. **Hermans, P. W. M., F. Abebe, V. I. O. Kuteyi, A. H. J. Kolk, J. E. R. Thole, and M. Harboe.** 1995. Molecular and immunological characterization of the highly conserved antigen 84 from *Mycobacterium tuberculosis* and *Mycobacterium leprae*. Infect. Immun. **63:**954–960.
21. **Hirota, Y., F. Jacob, A. Ryter, G. Buttin, and T. Nakai.** 1968. On the process of cellular division in *Escherichia coli*. I. Asymmetrical cell division and production of deoxyribonucleic acid-less bacteria. J. Mol. Biol. **35:**175–192.
22. **Honeyman, A. L., and G. C. Stewart.** 1989. The nucleotide sequence of the *rodC* operon of *Bacillus subtilis*. Mol. Microbiol. **3:**1257–1268.
23. **Lee, S., and C. W. Price.** 1993. The *minCD* locus of *Bacillus subtilis* lacks the *minE* determinant that provides topological specificity to cell division. Mol. Microbiol. **7:**601–610.
24. **Levin, P. A., and R. Losick.** 1994. Characterization of a cell division gene from *Bacillus subtilis* that is required for vegetative and sporulation septum formation. J. Bacteriol. **176:**1451–1459.
25. **Levin, P. A., and R. Losick.** 1996. Transcription factor Spo0A switches the localization of the cell division protein FtsZ from a medial to a bipolar pattern in *Bacillus subtilis*. Genes Dev. **10:**478–488.
26. **Levin, P. A., P. S. Margolis, P. Setlow, R. Losick, and D. Sun.** 1992. Identification of *Bacillus subtilis* genes for septum placement and shape determination. J. Bacteriol. **174:**6717–6728.
27. **Mendelson, N. H., and R. M. Cole.** 1972. Genetic regulation of cell division initiation in *Bacillus subtilis*. J. Bacteriol. **112:**994–1003.
28. **Nicholson, W. L., and P. Setlow.** 1990. Sporulation, germination, and outgrowth, p. 391–450. *In* C. R. Harwood and S. M. Cutting (ed.), Molecular biological methods for Bacillus. John Wiley & Sons, Chichester, United Kingdom.
29. **Pichoff, S., B. Vollrath, and J.-P. Bouche.** 1995. Deletion analysis of gene *minE* which encodes the topological specificity factor of cell division in *Escherichia coli*. Mol. Microbiol. **18:**321–330.

30. **Piggot, P. J., M. Amjad, J.-J. Wu, H. Sandoval, and J. Castro.** 1990. Genetic and physical maps of *Bacillus subtilis* 168, p. 493–543. *In* C. R. Harwood and S. M. Cutting (ed.), Molecular biological methods for Bacillus. John Wiley & Sons, Chichester, United Kingdom.
31. **Quinn, C. L., B. T. Stephenson, and R. L. Switzer.** 1991. Functional organization and nucleotide sequence of the *Bacillus subtilis* pyrimidine biosynthetic operon. J. Biol. Chem. **266:**9113–9127.
32. **Reeve, J. N., N. H. Mendelson, S. I. Coyne, L. L. Hallock, and R. M. Cole.** 1973. Minicells of *Bacillus subtilis*. J. Bacteriol. **114:**860–873.
33. **Rothfield, L. I., and C. R. Zhao.** 1996. How do bacteria decide where to divide? Cell **84:**183–186.
34. **Saito, H., and K. I. Miura.** 1963. Preparation of transferring deoxyribonucleic acid by phenol treatment. Biochim. Biophys. Acta **72:**619–629.
35. **Schaeffer, P., J. Millet, and J.-P. Aubert.** 1965. Catabolic repression of bacterial sporulation. Proc. Natl. Acad. Sci. USA **54:**704–711.
36. **Steinmetz, M., and R. Richter.** 1994. Plasmids designed to alter the antibiotic resistance expressed by insertion mutations in *Bacillus subtilis*, through in vivo recombination. Gene **142:**79–83.
37. **van Alstyne, D., and M. I. Simon.** 1971. Division mutants of *Bacillus subtilis*: isolation and PBS1 transduction of division-specific markers. J. Bacteriol. **108:**1366–1379.
38. **Vandeyar, M. A., and S. A. Zahler.** 1986. Chromosomal insertions of Tn*917* in *Bacillus subtilis*. J. Bacteriol. **167:**530–534.
39. **Varley, A. W., and G. C. Stewart.** 1992. The *divIVB* region of the *Bacillus subtilis* chromosome encodes homologs of *Escherichia coli* septum placement (MinCD) and cell shape (MreBCD) determinants. J. Bacteriol. **174:**6729–6742.
40. **Wachi, M., M. Doi, Y. Okada, and M. Matsuhashi.** 1989. New *mre* genes *mreC* and *mreD*, responsible for formation of the rod shape of *Escherichia coli* cells. J. Bacteriol. **171:**6511–6516.
41. **Wachi, M., and M. Matsuhashi.** 1989. Negative control of cell division by *mreB*, a gene that functions in determining the rod shape of *Escherichia coli* cells. J. Bacteriol. **171:**3123–3127.
42. **Wagner, P. M., and G. C. Stewart.** 1991. Role and expression of the *Bacillus subtilis rodC* operon. J. Bacteriol. **173:**4341–4346.
43. **Ward, J. E., Jr., and J. Lutkenhaus.** 1985. Overproduction of FtsZ induces minicell formation in *E. coli*. Cell **42:**941–949.
44. **Youngman, P., J. B. Perkins, and R. Losick.** 1984. A novel method for the rapid cloning in *Escherichia coli* of *Bacillus subtilis* chromosomal DNA adjacent to Tn*917* insertions. Mol. Gen. Genet. **195:**424–433.
45. **Zhao, C. R., P. A. J. de Boer, and L. I. Rothfield.** 1995. Proper placement of the *Escherichia coli* division site requires two functions that are associated with different domains of the MinE protein. Proc. Natl. Acad. Sci. USA **92:**4313–4317.